Nanoscale Advances

ROYAL SOCIETY OF CHEMISTRY

PAPER

Check for updates

Cite this: *Nanoscale Adv.*, 2021, **3**, 4528

Environmentally hazardous gas sensing ability of MoS_2-nanotubes: an insight from the electronic structure and transport properties†

Nabajyoti Baildya, *[a] Narendra Nath Ghosh [b] and Asoke P. Chattopadhyay [a]

Received 12th December 2020
Accepted 11th June 2021

DOI: 10.1039/d0na01037e

rsc.li/nanoscale-advances

Herein we have investigated the ability of the (6,6) MoS_2-nanotube (NT) to sense environmentally hazardous electrophilic and nucleophilic gases using density functional theory (DFT). CO, CO_2, H_2O and NH_3 gases were chosen for adsorption on the (6,6) MoS_2-NT and different adsorption parameters such as adsorption energy, projected density of states (PDOS), band structure and structural changes after adsorption were evaluated. Nucleophilic gases NH_3 and H_2O showed a fairly high amount of electron density transfer from gas molecules to the NT while the opposite trend was realized for electrophilic gases CO and CO_2. Among the four gases, H_2O has the highest amount of adsorption energy (−1.74 eV) and a moderately high amount of charge transfer from H_2O to the NT. Gas sensing behaviour was further rationalized from the enhanced *I*–*V* characteristics of gas adsorbed nanotubes compared to pristine ones. Analysis of results revealed that the (6,6) MoS_2-NT showed a decent level of gas sensing properties towards CO, CO_2, H_2O and NH_3 gases, and high selectivity for H_2O makes the MoS_2-NT superior to previously reported MoS_2-monolayer in this matter. These results suggest the possibility of fabrication of highly efficient MoS_2-NT based gas sensors for environmentally hazardous gases.

Introduction

Toxic and carcinogenic gases are the main contributors to air pollution. These gases can affect both human health and the environment directly or indirectly. Oxides of carbon, nitrogen and other elements, along with methane, ammonia, CFCs and water vapour in air are mainly responsible for air pollution leading to various pulmonary and other diseases. Global warming is another issue which we cannot ignore any more. In this context, gas sensors which are cost effective, easy to use and require low power to operate are very promising candidates. Lots of research endeavours to discover and design such efficacious gas sensing materials are being carried out.

Use of 2D-materials such as graphene, hexagonal boron nitride nanosheets and carbon NTs as gas sensing agents is decades old.[1–4] Graphene oxide can also be used as a gas sensor.[5] Graphene quantum dots have shown potential sensing ability for toxic gases.[6] In the last few years, 2D-materials of transition metal dichalcogenides (TMDs) *viz.* MX_2 (X = S, Se, Te) have drawn attention due to their potential gas sensing properties.[7] Among these TMDs, MoS_2 has gas sensing ability comparable to graphene[8,9] and WS_2 can sense both toxic and non-toxic gases.[10,11]

Among the 2D-transition metal dichalcogenides (TMDs), MoS_2 has evoked keen interest to the researchers due to its use in various fields *e.g.* optics, microbiology, catalysis, electrical appliances, energy conversion, gas sensing and lubrication.[7,12–17] Both bulk and single-layer MoS_2 showed semiconducting nature with an indirect band gap of 1.23 eV and 1.8 eV, respectively.[18,19] In MoS_2, the Mo-atom is sandwiched between two S-atoms through covalent bonds, while the monolayers are held together by weak van der Waals forces.[20] MoS_2 monolayer plays a key role in adsorbing and detecting gases such as NH_3, NO, NO_2, CO, H_2O, CO_2, CH_4, *etc.*7–9, which are hazardous to both the environment and human health. The adsorption behaviour of MoS_2 monolayer is also explained by measuring the electronic transport properties of gas adsorbed MoS_2 monolayer. The gas sensing ability of MoS_2@gas monolayer is explained by changes in the rectification behaviour.[11] The adsorption of CO and H_2 gases on MoS_2 monolayer by creating sulphur vacancies, *i.e.* by defective MoS_2 monolayer, results in enhanced catalytic activity.[20] The adsorption power of MoS_2 monolayer was found to be enhanced by silver functionalization.[21] Transition metal (V, Nb, Ta, and Ni) doped MoS_2 monolayer additionally showed potential gas adsorption properties.[22,23] The effect of applied electric field on gas sensing by MoS_2 monolayer has also been reported.[24]

Semiconducting MoS_2-NTs have a graphitic honeycomb structure. Single walled MoS_2-NTs can be synthesized by

[a]*Department of Chemistry, University of Kalyani, Kalyani 741235, India. E-mail: nabajyotibaildya@gmail.com; asoke@klyuniv.ac.in*

[b]*Department of Chemistry, University of Gour Banga, Mokdumpur, Malda, 732103, India. E-mail: ghosh.naren13@gmail.com*

† Electronic supplementary information (ESI) available. See DOI: 10.1039/d0na01037e

This article is licensed under a Creative Commons Attribution-NonCommercial 3.0 Unported Licence.

(cc) BY-NC

© 2021 The Author(s). Published by the Royal Society of Chemistry

heating ammonium thiomolybdate[25] or by applying the catalytic transport of C_{60} with MoS_2 powder.[26] It has generally two forms: (i) armchair (n,n) and (ii) zigzag (n,0).[24] Among these two forms, the armchair (n,n) MoS_2-NT shows an indirect band gap whereas the zigzag form shows a direct band gap. For the (n,n) MoS_2-NT, the band gap increases with the increase in the magnitude of n.[27] MoS_2-NT systems can sense NH_3 and NO_2 gases.[28] There are several reports on the variation of gas sensing properties of MoS_2-monolayer along with some other TMD materials, but the atomistic description of gas sensing ability of MoS_2-NTs is scarce.[5,29,30] In the present work, we have made a comprehensive analysis of the adsorption behaviour and gas sensing ability of the (6,6) MoS_2-NT. Compared to other armchair (8,8; 10,10; 12,12; 14,14 with band gaps of 0.496, 0.783, 0.954, and 1.079 eV, respectively) and zig-zag (10,0; 12,0; 14,0 with band gaps of 0.225, 0.405, and 0.615 eV, respectively) MoS_2-NTs, the (6,6) NT possesses a lower band gap (0.19 eV).[27] So modulation of the electronic properties by adsorption of different gases can be achieved more easily involving the (6,6) NT. Furthermore, the results of adsorption of CO, CO_2, NH_3 and H_2O on the (6,6) MoS_2-NT are compared to those on 2D MoS_2-monolayer (ML). Surprisingly, it was found that the MoS_2-NT can act as a better gas sensing agent as compared to MoS_2-monolayer. This is verified from the binding energy analysis and explained by changes in the physical and electronic structure and *I–V* characteristics of the gases after adsorption.

Methodology

In the present work, the (6,6) MoS_2 armchair NT has been chosen for the adsorption of CO, CO_2, NH_3 and H_2O gases. A double-ζ plus (DZP) function basis set and a mesh cut-off of 300 Ry at 300 K electronic temperature were considered for geometry optimization. The Perdew–Burke–Ernzerhof (PBE)[31] type generalized gradient approximation (GGA) exchange-correlation functional is used in all calculations, as implemented in the SIESTA program suite.[32,33] Though the PBE functional underestimates the band gap, the results offered by the PBE functional are quite reasonable and cost effective as demonstrated by previous reports.[34,35] The density matrix convergence criterion is set at 10^{-4}. The conjugate gradient method is used to stabilize all atoms until the maximum tolerance force reached a value less than 0.01 eV $Å^{-1}$. A $1 \times 1 \times 6$ Monkhorst–Pack k-grid with a vacuum more than 20 Å in the x and y directions is applied in order to decouple the adjacent mirror images. In the present study, a single gas molecule was considered for adsorption on the NT to avoid spurious interactions between two neighbouring adsorbate gases. The adsorption energies of the gases are calculated using the following equation:

$$E_{ads.} = E_{nanotube+gas} - E_{nanotube} - E_{gas} \quad (1)$$

where $E_{nanotube+gas}$ indicates the total energy of the composite system and $E_{nanotube}$ and E_{gas} are the energies of the MoS_2-NT and the studied gases, respectively.

Furthermore, to understand the adsorption mechanism, electronic transport properties of the MoS_2-NT and MoS_2-NT@gases have been studied by applying density functional theory combined with non-equilibrium Green's function as implemented in TranSIESTA.[34] A similar correlation functional was used to calculate the transport properties as above. To study the transport properties of the MoS_2-NT and MoS_2-NT@gas, three regions were considered *viz.* the left hand electrode (LHE,

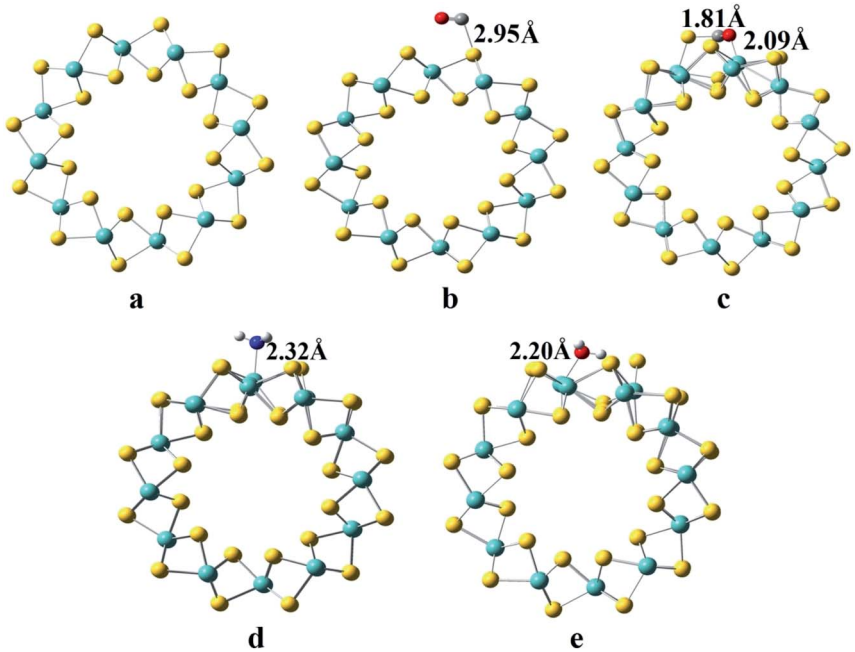

Fig. 1 Top view of the MoS_2-NT and gas adsorbed MoS_2-NT (a) MoS_2-NT, (b) MoS_2-NT@CO, (c) MoS_2-NT@CO_2, (d) MoS_2-NT@NH_3, and (e) MoS_2-NT@H_2O.

© 2021 The Author(s). Published by the Royal Society of Chemistry

containing 36 atoms), right hand electrode (RHE, containing 36 atoms) and scattering region (SR, containing 140 atoms in the MoS_2-NT, 142 atoms in MoS_2-NT@CO, 143 atoms in MoS_2-NT@CO_2, 144 atoms in MoS_2-NT@NH_3 and 143 atoms in MoS_2-NT@H_2O). Applying the Landauer–Buttiker formula under finite bias (V_b), the amount of current passed was calculated within the energy bias window from $-eV_b/2$ to $+eV_b/2$ by integrating the transmission function $T(E, V_b)$.

$$I(V_b) = \frac{2e}{h}\int_{-\infty}^{+\infty} T(E,\ V_b)[f_L(E-\ \mu_L) - f_R(E-\ \mu_R)]\mathrm{d}E \quad (2)$$

where f_L and f_R are the Fermi–Dirac distribution functions for the left and right electrodes, respectively and μ_L and μ_R are the chemical potentials of the left and right electrodes, respectively and $eV_b = \mu_L - \mu_R$. To understand the *I vs. V* characteristics, a finite bias from −1 to 1 V was used keeping a bias spacing of 0.1 eV.

Results and discussion

The optimized lattice parameter for the (6,6) MoS_2-NT was found to be 3.23 Å, which is much better than that found in previous theoretical studies.[27] Optimized structures of the (6,6) MoS_2-NT itself and with CO, CO_2, H_2O and NH_3 adsorbed on it are shown in Fig. 1a–e. Four different adsorption sites *viz.* the top of the hexagon (the H-site), top of the outer S-atom (the S-site), top of the Mo-atom (the M-site) and top of a Mo–S bond site (the B-site) on the surface of the MoS_2-NT were considered for gas adsorption. We note that for CO and CO_2 adsorption, the preferable sites are the H-site and S-site, respectively, while for NH_3 and H_2O the preferable site is the M-site.

Fig. 2a shows the adsorption energies of the composite systems along with the favoured binding sites (values are available in Table S1†). The MoS_2-NT@CO system has an adsorption energy of −0.44 eV at the H-site; for the MoS_2-

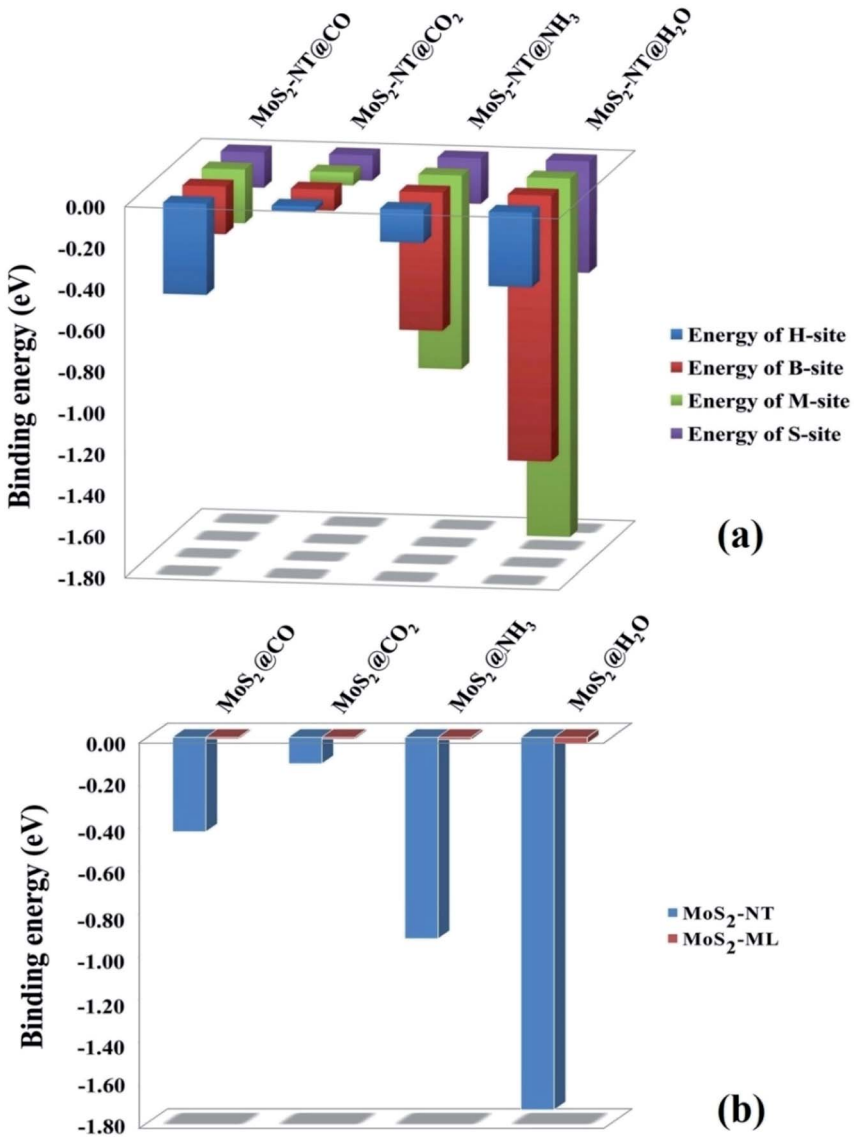

Fig. 2 (a) Adsorption energies of gases at different sites of the MoS_2-NT, (b) adsorption energies of gases with the MoS_2-NT and MoS_2-ML.[7]

© 2021 The Author(s). Published by the Royal Society of Chemistry

NT@CO_2 system, the adsorption energy at the S-site is −0.12 eV and for MoS_2-NT@NH_3 and MoS_2-NT@H_2O, where adsorption is on the M-site, the adsorption energy values are −0.94 eV and −1.74 eV, respectively.

The negative adsorption energies reveal that the adsorption is purely exothermic and therefore energetically favourable in all cases. Fig. 2b shows the comparison of adsorption energies between the MoS_2-NT and MoS_2-monolayer (ML)[7] which clearly indicates that the MoS_2-NT shows greater adsorption energies compared to MoS_2-ML (adsorption energies are given in Table S2, ESI†).

From the above figure, it is clear that the nucleophilic gases NH_3 and H_2O are adsorbed more strongly on the (6,6) MoS_2-NT yielding higher adsorption energies, while the electrophilic gases CO and CO_2 are less strongly adsorbed with lower adsorption energies. Analysis of bond lengths and adsorption energies revealed that the nucleophilic gases are adsorbed preferentially over the electrophilic sites on the (6,6) MoS_2-NT, while electrophilic gases prefer to bind to the nucleophilic sites more. The bond distances of CO and CO_2 from their nearest sulphur atom of the MoS_2-NT are 2.95 Å and 2.82 Å, respectively, while the bond distances of NH_3 and H_2O from their nearest Mo atom are 2.32 Å and 2.20 Å, respectively. Higher values of adsorption energies of the nucleophilic gases are also understood from the Mulliken charge analysis. Fig. 3 enlists the Mulliken charges of the composite systems studied (data are listed in Table S3, ESI†).

It was found that, for NH_3 and H_2O, 0.25 and 0.08 electronic charges were respectively transferred to the MoS_2-NT on adsorption. However, 0.08 and 0.07 electronic charges were transferred from the MoS_2-NT to the anti-bonding π^*-orbital of CO and CO_2 gases, respectively. The charge transfer from the MoS_2-NT to CO and CO_2 is further understood from the elongation of the C–O bond from 1.14 Å to 1.15 Å in CO and from 1.17 Å to 1.28 Å in CO_2 as these gases are adsorbed on the MoS_2-NT. Similarly, the charge transfer from MoS_2 to NH_3 and H_2O is further evident from the elongation of the N–H bond from 1.02 Å to 1.03 Å in NH_3 and of the O–H bond from 0.97 Å to 1.02 Å in H_2O along with the change in the bond angle in both NH_3 and H_2O molecules, as these are adsorbed on the MoS_2-NT.

The valence band maxima (VBM) and conduction band minima (CBM) of the composite systems are in accordance with the Mulliken charge analysis. Fig. 4 shows how the electrophilic and nucleophilic character of the gases affect the charge transfer from the MoS_2-NT to gases and *vice versa*. The charge density distribution shown in Fig. 4 clearly demonstrates that a substantial amount of electron density is transferred from the NT to electrophilic CO and CO_2 while for NH_3 and H_2O a reverse trend is observed.

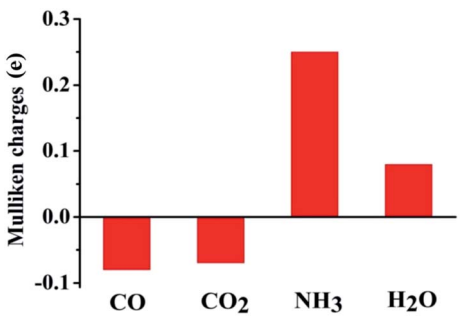

Fig. 3 Mulliken charges on gases adsorbed on the MoS_2-NT.

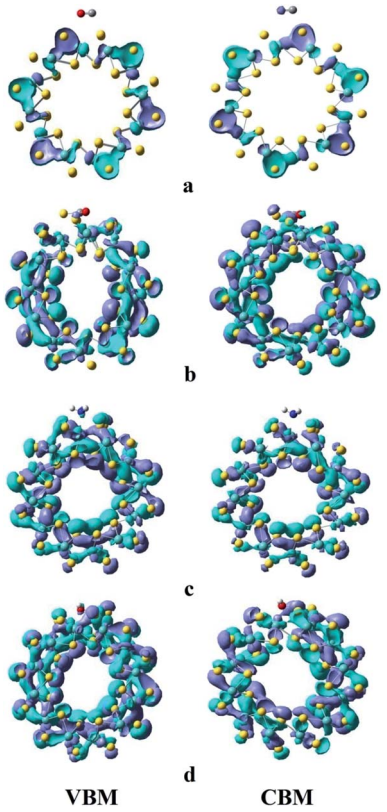

Fig. 4 Charge density isosurface (isovalue = 0.02) plot for MoS_2-NT@gases: (a) MoS_2-NT–CO, (b) MoS_2-NT–CO_2, (c) MoS_2-NT–NH_3, and (d) MoS_2-NT–H_2O.

Structural parameters of these gases before and after adsorption are presented in Table 1. The obtained results revealed a significant change in the structure of the gases after adsorption on the (6,6) MoS_2-NT. Bond lengths of all gases are increased upon adsorption on the NT. Bond angles are also increased in CO_2, NH_3 and H_2O after adsorption. For CO and CO_2, the bond lengths are increased by 0.01 Å and 0.11 Å, respectively, along with a change in the bond angle from 179.94° to 119.32° in the case of CO_2. In the case of NH_3 and H_2O, the bond lengths are increased by 0.01 Å and 0.05 Å, respectively, and the bond angles are increased by 2.40° and 0.75°, respectively, after adsorption.

The projected density of states (PDOS) of different gases adsorbed on the MoS_2-NT is plotted in Fig. 5a–e to analyse the contribution arising from the gases and the MoS_2-NT to the corresponding valence and conduction bands of the composite systems. It must be noted that the more electronegative S atom appears in the valence band while the more electropositive Mo atom contributes to the conduction band of the MoS_2-NT. Furthermore, compared to the free MoS_2-NT, the composite

© 2021 The Author(s). Published by the Royal Society of Chemistry

Table 1 Structural changes of gases after adsorption on the MoS_2-NT

Gas	Bond length in free gas (Å)	Bond angle in free gas (degree)	Bond length in adsorbed gas (Å)	Bond angle in adsorbed gas (degree)
CO	1.14	—	1.15	—
CO_2	1.17	179.94	1.28	119.32
NH_3	1.02	107.49	1.03	109.89
H_2O	0.97	104.89	1.02	105.64

systems showed smaller band gaps. The nucleophilic NH_3 and H_2O gases appear in the corresponding conduction band of the composite system due to the transfer of electron density from the gases to the conduction band of the MoS_2-NT. With electrophilic gases, there is a significant charge transfer from the more electronegative sulphur of the MoS_2-NT to the corresponding vacant orbital of the CO and CO_2 gases, resulting in the elongation of the C–O bond (bond length 1.14 to 1.15 Å) in CO while a change in hybridization from sp to sp^2 in CO_2.

To analyze the performance of the MoS_2-NT as a potential sensor, the non-equilibrium Green's function (NEGF) method is employed to evaluate the transport and corresponding current–voltage (*I–V*) characteristics of the MoS_2-NT before and after gas adsorption. The model systems of the designed two semi-infinite electrodes along with the scattering region where the different gases were adsorbed are shown in Fig. 6.

A remarkable effect of gas adsorption on current–voltage characteristics is observed from the *I vs. V* curve as presented in Fig. 7. For all gas adsorption cases, *I vs. V* showed a noticeable increase in current flow with respect to the pristine MoS_2-NT. This increase in the current signal clearly indicates that there is a huge impact on the transport characteristics of the MoS_2-NT after gas adsorption. Among the four different gas adsorption cases, the CO_2 adsorbed MoS_2-NT showed enhanced current flow. However NH_3 and CO adsorbed MoS_2-NTs showed almost a similar current flow, and the H_2O adsorbed MoS_2-NT showed the least current flow. A similar effect of NH_3 and CO adsorbed MoS_2-NTs can be attributed to the similarity of the energy difference between the conduction and valence bands. On the other hand, the stronger effect of CO_2 adsorption on the transport characteristics can be explained from the large decrease of the CBM and VBM energy states. It is interesting to note that, though H_2O is strongly adsorbed on the MoS_2-NT (−1.74 eV) and there is a large decrease in the CBM and VBM levels, current flow is least affected by H_2O adsorption. Such current–voltage behaviour for H_2O and CO_2 adsorption can be

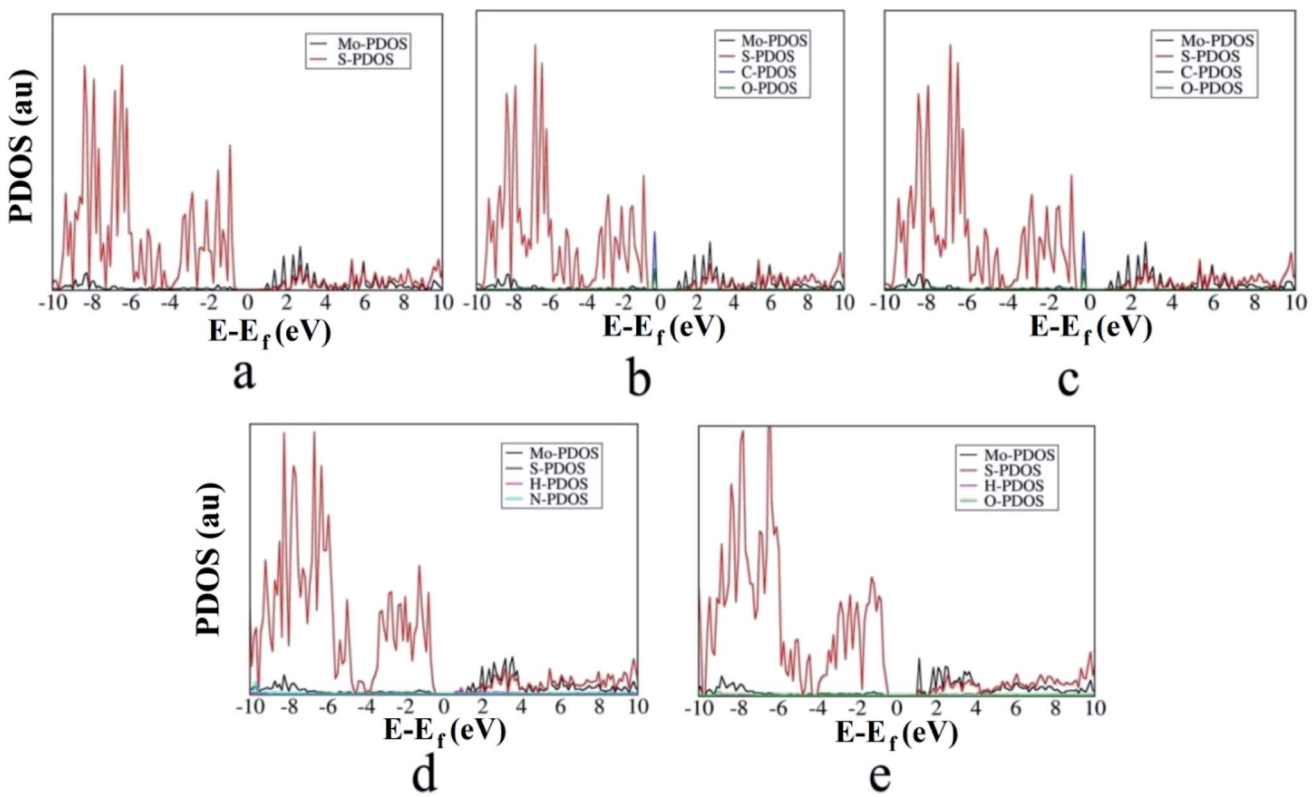

Fig. 5 PDOS of the (6,6) MoS_2-NT and MoS_2-NT@gases: (a) MoS_2-NT, (b) MoS_2-NT@CO, (c) MoS_2-NT@CO_2, (d) MoS_2-NT@NH_3 and (e) MoS_2-NT@H_2O.

© 2021 The Author(s). Published by the Royal Society of Chemistry

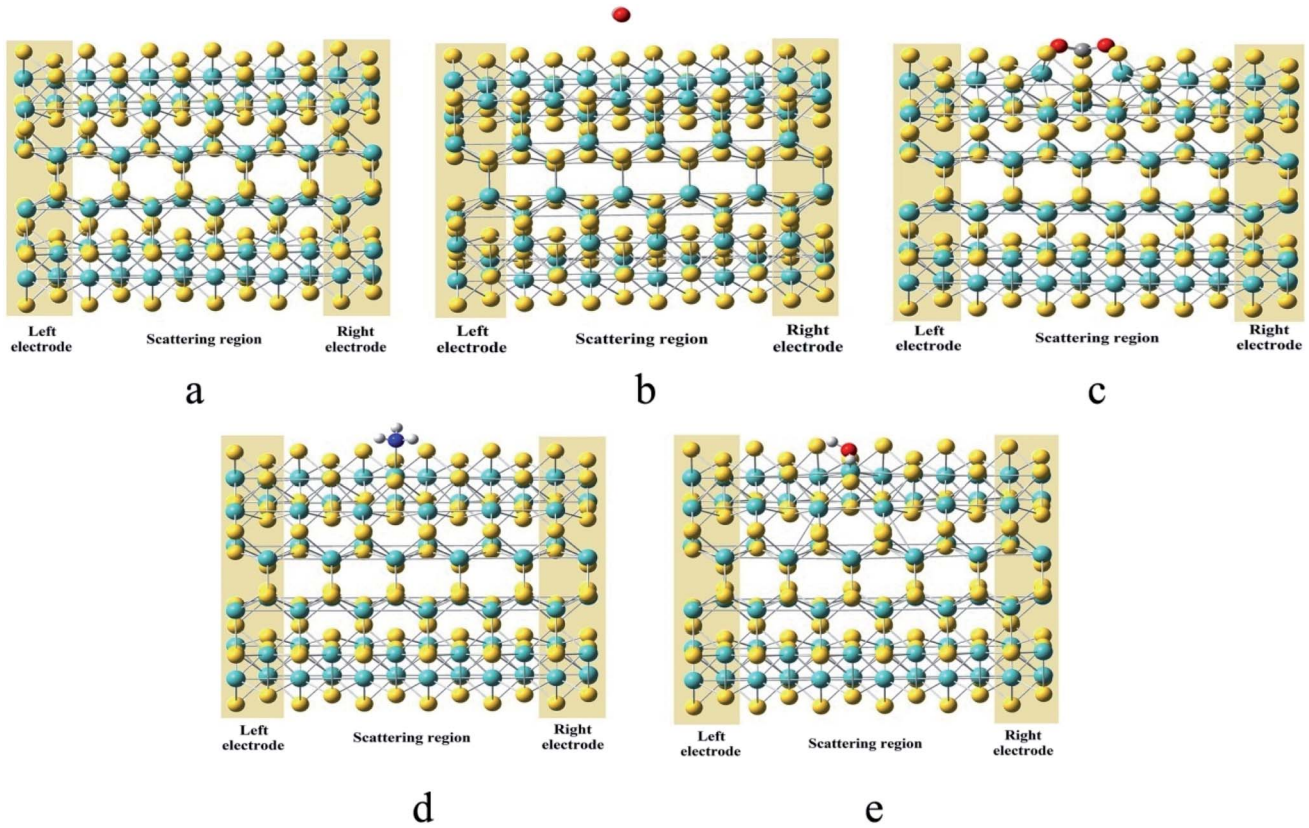

Fig. 6 Optimised geometries of (a) the MoS_2-NT, (b) MoS_2-NT@CO, (c) MoS_2-NT@CO_2, (d) MoS_2-NT@NH_3, and (e) MoS_2-NT@H_2O with electrodes and the scattering region.

interpreted by the inhibition of the conduction channel due to an appreciable amount of charge flow from H_2O to the MoS_2-NT.

The noticeable difference in the current signal due to gas adsorption can be regarded as a superior characteristic of the device modelling of MoS_2-NT based gas sensors.

To better understand the shifting of conduction and valence bands due to charge transfer after adsorption of gases, we have plotted the transmission function for bare and adsorbed NTs as shown in Fig. 8. Charge transfer in MoS_2-NT@CO_2 from the MoS_2-NT to CO_2 results in the shrinking of the transport bands and the transmission function shows a broad peak in conduction and valence bands. As a result, CO_2 adsorption increases the conduction channel in MoS_2-NT@CO_2, showing a broad current signal in the *I vs. V* window. On the other hand, charge transfer from H_2O to the MoS_2-NT shifts the conduction band to a lower energy, thereby inhibiting the conduction channel which shows lower transmission peaks. A similar behaviour in the current signal in the *I vs. V* window for MoS_2-NT@NH_3 and MoS_2-NT@CO has been attributed to the alignment of similar transport bands and transmission signals in valence and conduction bands.

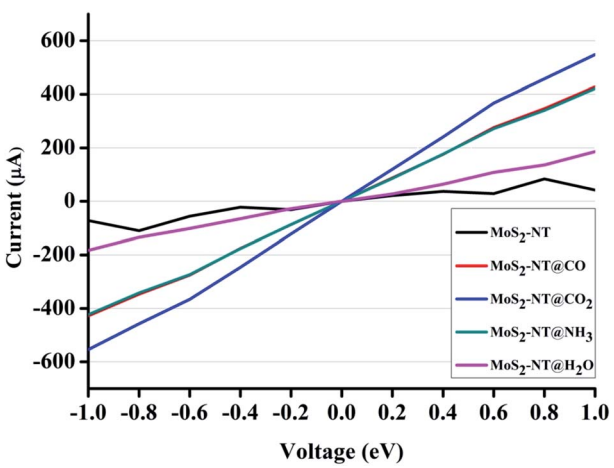

Fig. 7 *I vs. V* characteristics of the MoS_2-NT, MoS_2-NT@CO, MoS_2-NT@CO_2, MoS_2-NT@NH_3 and MoS_2-NT@H_2O.

Furthermore, to understand how adsorption affects the overall band structure of these systems, we have performed band structure analysis of the MoS_2-NT and gas adsorbed MoS_2-NT as shown in Fig. 9a–e. Fig. 9a revealed an indirect band gap of 0.19 eV for the free MoS_2-NT. After gas adsorption, there is a profound impact on the band structure of the system.

After adsorption of different gases, the indirect band gap decreases in all cases. For MoS_2-NT@CO, the band gap is 0.13 eV and for MoS_2-NT@CO_2, this band gap is reduced further to 0.04 eV. Again, in MoS_2-NT@NH_3, the band gap is 0.15 eV and for MoS_2-NT@H_2O, there is an overlap between the valence and conduction bands. For MoS_2-NT@CO and MoS_2-NT@CO_2, the conduction bands become more dense compared to those of

© 2021 The Author(s). Published by the Royal Society of Chemistry

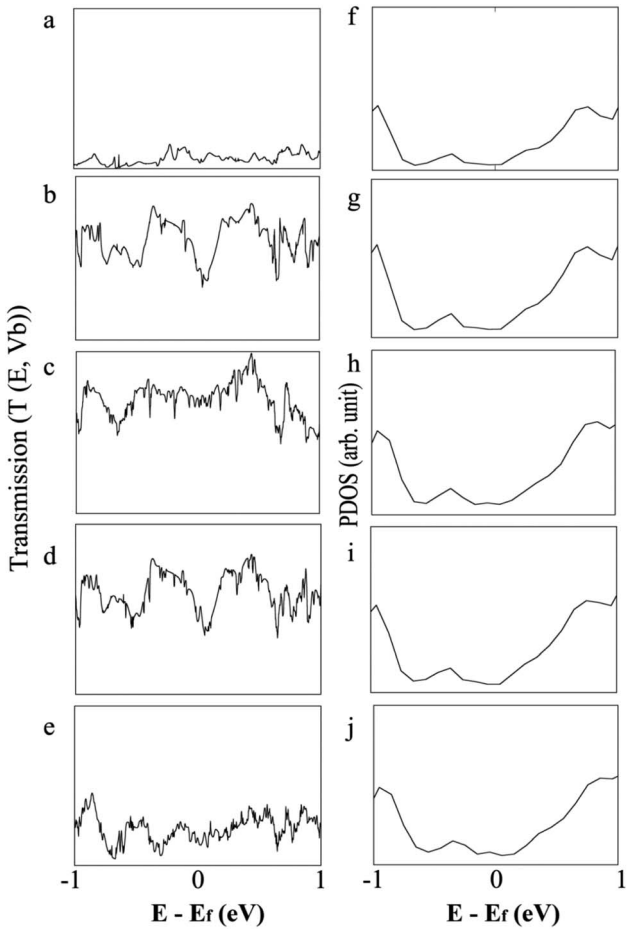

Fig. 8 Transmission function of (a) the MoS_2-NT, (b) MoS_2-NT@CO, (c) MoS_2-NT@CO_2, (d) MoS_2-NT@NH_3, (e) MoS_2-NT@H_2O and PDOSs of (f) the MoS_2-NT, (g) MoS_2-NT@CO, (h) MoS_2-NT@CO_2, (i) MoS_2-NT@NH_3, (j) MoS_2-NT@H_2O.

MoS_2-NT. Furthermore, in the case of MoS_2-NT@NH_3 and MoS_2-NT@H_2O, the density of the conduction band is increased further. Hence the band structure is also in concordance with the Mulliken charge analysis and VBM-CBM analysis. Only in the case of MoS_2-NT@H_2O, the conduction band crosses the Fermi level, which is an indication of the metallic character of the system. It is also clear from the band structure that the MoS_2-NT shows much stronger binding with H_2O. Thus the band structures also explain the binding nature of the gases on the MoS_2-NT.

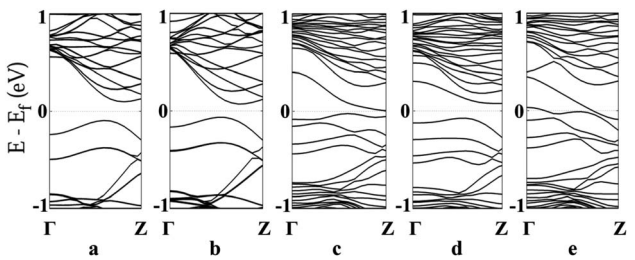

Fig. 9 Band structure of the MoS_2-NT and MoS_2-NT@gases: (a) MoS_2-NT, (b) MoS_2-NT@CO, (c) MoS_2-NT@CO_2, (d) MoS_2-NT@NH_3 and (e) MoS_2-NT@H_2O.

Conclusions

In the present work, the adsorption of environmentally hazardous gases on the (6,6)-MoS_2-NT was analysed from their electronic structure and transport properties. Binding is controlled by the electrophilic and nucleophilic characters of the gases, which also govern charge transfer to and from the MoS_2-NT. The electrophilic character of CO and CO_2 lead to charge transfer from the NT to these gases, whereas the nucleophilic character of NH_3 and H_2O showed the reverse trend. These gases, upon adsorption on the MoS_2-NT, are activated, as evident from the structural changes in these gases. These phenomena are explained by Mulliken charge analysis, VBM-CBM analysis, *I vs. V* characteristics, transmission function, PDOS and band structure analysis. The presence of more electronegative atoms on the molecule also controls the binding energy and the band structure of the systems studied. Analysis of data reveals that compared to MoS_2-ML, the MoS_2-NT showed enhanced gas sensing ability and distinct *I–V* characteristics, which suggests the fabrication of new gas sensing devices from the MoS_2 based NT.

Data availability

Data are available upon request to the corresponding author.

Author contributions

Nabajyoti Baildya: conceptualization, planning, writing. Narendra Nath Ghosh: conceptualization, execution, writing. Asoke P. Chattopadhyay: planning, supervision, writing.

Conflicts of interest

The authors declare no conflicting interest among themselves regarding the present work.

Acknowledgements

The authors wish to acknowledge infrastructural support from the Department of Chemistry, University of Kalyani, Kalyani, Nadia, India.

References

1 K. S. Novoselov, D. Jiang, F. Schedin, T. Booth, V. Khotkevich, S. Morozov and A. K. Geim, Two-dimensional atomic crystals, *Proc. Natl. Acad. Sci. U. S. A.*, 2005, **102**(30), 10451–10453.

2 C. Lee, Q. Li, W. Kalb, X.-Z. Liu, H. Berger, R. W. Carpick and J. Hone, Frictional characteristics of atomically thin sheets, *science*, 2010, **328**(5974), 76–80.

3 L. Ci, L. Song, C. Jin, D. Jariwala, D. Wu, Y. Li, A. Srivastava, Z. Wang, K. Storr and L. Balicas, Atomic layers of hybridized

© 2021 The Author(s). Published by the Royal Society of Chemistry

boron nitride and graphene domains, *Nat. Mater.*, 2010, **9**(5), 430–435.
4 Y. Wang and J. T. Yeow, A review of carbon nanotubes-based gas sensors, *J. Sens.*, 2009, 2009.
5 M. Donarelli and L. Ottaviano, 2D materials for gas sensing applications: A review on graphene oxide, MoS_2, WS_2 and phosphorene, *Sensors*, 2018, **18**(11), 3638.
6 D. Raeyani, S. Shojaei and S. AhmadiKandjani, Optical graphene quantum dots gas sensors: experimental study, *Mater. Res. Express*, 2020, **7**(1), 015608.
7 S. Zhao, J. Xue and W. Kang, Gas adsorption on MoS_2 monolayer from first-principles calculations, *Chem. Phys. Lett.*, 2014, **595**, 35–42.
8 B. Cho, J. Yoon, S. K. Lim, A. R. Kim, D.-H. Kim, S.-G. Park, J.-D. Kwon, Y.-J. Lee, K.-H. Lee and B. H. Lee, Chemical sensing of 2D graphene/MoS_2 heterostructure device, *ACS Appl. Mater. Interfaces*, 2015, **7**(30), 16775–16780.
9 J. Ren, H. Liu, Y. Xue and L. Wang, Adsorption Behavior of CH 4 Gas Molecule on the MoX 2 (S, Se, Te) Monolayer: The DFT Study, *Nanoscale Res. Lett.*, 2019, **14**(1), 293.
10 V. Babar, H. Vovusha and U. Schwingenschlögl, Density Functional Theory Analysis of Gas Adsorption on Monolayer and Few Layer Transition Metal Dichalcogenides: Implications for Sensing, *ACS Appl. Nano Mater.*, 2019, **2**(9), 6076–6080.
11 J. Sun, N. Lin, H. Ren, C. Tang, L. Yang and X. Zhao, Gas adsorption on MoS_2/WS_2 in-plane heterojunctions and the I–V response: a first principles study, *RSC Adv.*, 2016, **6**(21), 17494–17503.
12 E. Gourmelon, O. Lignier, H. Hadouda, G. Couturier, J. Bernède, J. Tedd, J. Pouzet and J. Salardenne, MS2 (M= W, Mo) photosensitive thin films for solar cells, *Sol. Energy Mater. Sol. Cells*, 1997, **46**(2), 115–121.
13 V. Yadav, S. Roy, P. Singh, Z. Khan and A. Jaiswal, 2D MoS_2-based nanomaterials for therapeutic, bioimaging, and biosensing applications, *Small*, 2019, **15**(1), 1803706.
14 T. F. Jaramillo, K. P. Jørgensen, J. Bonde, J. H. Nielsen, S. Horch and I. Chorkendorff, Identification of active edge sites for electrochemical H2 evolution from MoS_2 nanocatalysts, *science*, 2007, **317**(5834), 100–102.
15 Y. Li, H. Wang, L. Xie, Y. Liang, G. Hong and H. Dai, MoS_2 nanoparticles grown on graphene: an advanced catalyst for the hydrogen evolution reaction, *J. Am. Chem. Soc.*, 2011, **133**(19), 7296–7299.
16 B. Radisavljevic, A. Radenovic, J. Brivio, V. Giacometti and A. Kis, Single-layer MoS 2 transistors, *Nat. Nanotechnol.*, 2011, **6**(3), 147–150.
17 W. Wu, L. Wang, Y. Li, F. Zhang, L. Lin, S. Niu, D. Chenet, X. Zhang, Y. Hao and T. F. Heinz, Piezoelectricity of single-atomic-layer MoS 2 for energy conversion and piezotronics, *Nature*, 2014, **514**(7523), 470–474.
18 K. Kam and B. Parkinson, Detailed photocurrent spectroscopy of the semiconducting group VIB transition metal dichalcogenides, *J. Phys. Chem.*, 1982, **86**(4), 463–467.
19 K. F. Mak, C. Lee, J. Hone, J. Shan and T. F. Heinz, Atomically thin MoS_2: a new direct-gap semiconductor, *Phys. Rev. Lett.*, 2010, **105**(13), 136805.
20 D. Le, T. B. Rawal and T. S. Rahman, Single-layer MoS_2 with sulfur vacancies: structure and catalytic application, *J. Phys. Chem. C*, 2014, **118**(10), 5346–5351.
21 J. Song and H. Lou, Improvement of gas-adsorption performances of Ag-functionalized monolayer MoS_2 surfaces: A first-principles study, *J. Appl. Phys.*, 2018, **123**(17), 175303.
22 H. Wei, Y. Gui, J. Kang, W. Wang and C. Tang, A DFT study on the adsorption of H_2S and SO_2 on Ni doped MoS_2 monolayer, *Nanomaterials*, 2018, **8**(9), 646.
23 Q. Yue, Z. Shao, S. Chang and J. Li, Adsorption of gas molecules on monolayer MoS_2 and effect of applied electric field, *Nanoscale Res. Lett.*, 2013, **8**(1), 425.
24 G. Seifert, H. Terrones, M. Terrones, G. Jungnickel and T. Frauenheim, Structure and electronic properties of MoS 2 nanotubes, *Phys. Rev. Lett.*, 2000, **85**(1), 146.
25 M. Nath, A. Govindaraj and C. N. R. Rao, Simple synthesis of MoS_2 and WS_2 nanotubes, *Adv. Mater.*, 2001, **13**(4), 283–286.
26 M. Remskar, A. Mrzel, Z. Skraba, A. Jesih, M. Ceh, J. Demšar, P. Stadelmann, F. Lévy and D. Mihailovic, Self-assembly of subnanometer-diameter single-wall MoS_2 nanotubes, *Science*, 2001, **292**(5516), 479–481.
27 R. Ansari, S. Malakpour, M. Faghihnasiri and S. Sahmani, An *ab initio* investigation into the elastic, structural and electronic properties of MoS_2 nanotubes, *Superlattices Microstruct.*, 2015, **82**, 188–200.
28 G. Deokar, P. Vancso, R. Arenal, F. Ravaux, J. Casanova-Cháfer, E. Llobet, A. Makarova, D. Vyalikh, C. Struzzi and P. Lambin, MoS_2–carbon nanotube hybrid material growth and gas sensing, *Adv. Mater. Interfaces*, 2017, **4**(24), 1700801.
29 Y. Niu, R. Wang, W. Jiao, G. Ding, L. Hao, F. Yang and X. He, MoS_2 graphene fiber based gas sensing devices, *Carbon*, 2015, **95**, 34–41.
30 S. Cui, Z. Wen, X. Huang, J. Chang and J. Chen, Stabilizing MoS_2 nanosheets through SnO_2 nanocrystal decoration for high-performance gas sensing in air, *Small*, 2015, **11**(19), 2305–2313.
31 J. P. Perdew, K. Burke and M. Ernzerhof, Generalized gradient approximation made simple, *Phys. Rev. Lett.*, 1996, **77**(18), 3865.
32 E. Artacho, E. Anglada, O. Diéguez, J. D. Gale, A. García, J. Junquera, R. M. Martin, P. Ordejón, J. M. Pruneda and D. Sánchez-Portal, The SIESTA method; developments and applicability, *J. Phys.: Condens. Matter*, 2008, **20**(6), 064208.
33 J. M. Soler, E. Artacho, J. D. Gale, A. García, J. Junquera, P. Ordejón and D. Sánchez-Portal, The SIESTA method for *ab initio* order-N materials simulation, *J. Phys.: Condens. Matter*, 2002, **14**(11), 2745.
34 G. Sivaraman, F. b. A. de Souza, R. G. Amorim, W. L. Scopel, M. Fyta and R. H. Scheicher, Electronic transport along hybrid MoS_2 monolayers, *J. Phys. Chem. C*, 2016, **120**(41), 23389–23396.
35 P. Bonardi, S. Achilli, G. F. Tantardini and R. Martinazzo, Electron transport in carbon wires in contact with Ag electrodes: a detailed first principles investigation, *Phys. Chem. Chem. Phys.*, 2015, **17**(28), 18413–18425.

© 2021 The Author(s). Published by the Royal Society of Chemistry